5 Experimental work

5.1 Experimental setup

The experimental apparatus was already constructed when I began my research, and has been described in a paper and thesis by Dr. Lance Christensen.[1,2] This chapter provides more details on the operating conditions of the apparatus during the work presented in Chapters 2 and 4, and describes experiments conducted to further characterize the apparatus. **Figure 5-1** presents a schematic overview of the setup.

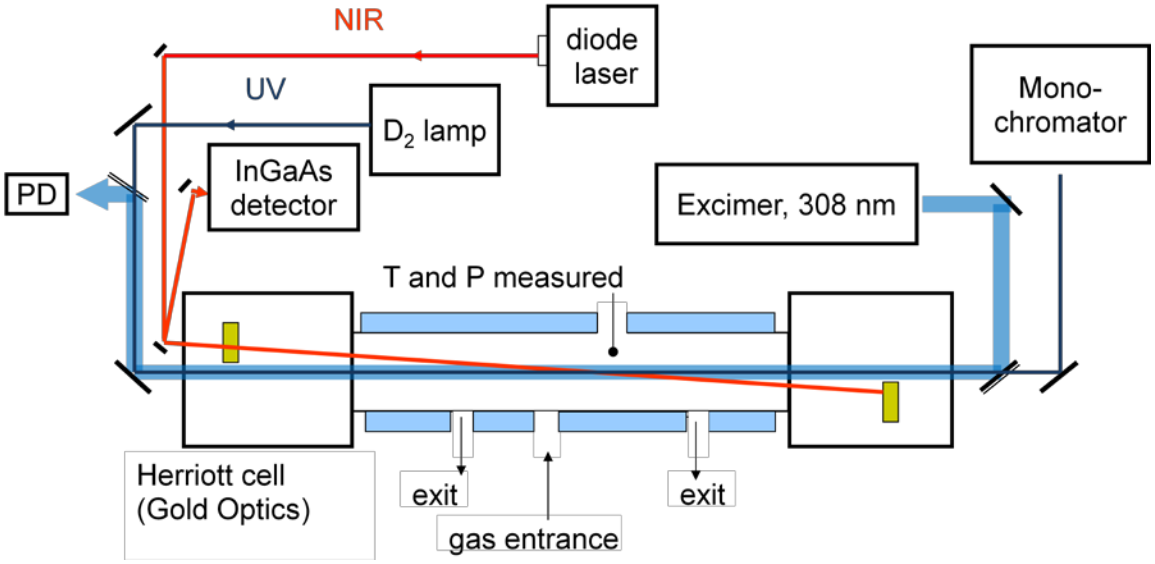

Figure 5-1. IRKS apparatus. A jacketed flow cell is coupled to an excimer laser for flash photolysis kinetics experiments. Two detection probes, near-IR light from a diode laser and UV light from a deuterium lamp are monitored simultaneously. The NIR probe makes 30 passes back and forth through the cell using Herriott mirrors slightly off axis to the photolysis pulse. The UV probe is coaligned, but propagating in the opposite direction of the photolysis pulse.

The main glass cell was jacketed to allow for temperature control using liquid-nitrogen-chilled methanol as a coolant. The cell was connected with O-ring seals to mirror housing boxes on either end where the near infrared (NIR) Herriott cell mirrors were located. Calcium fluoride (CaF_2) windows on the boxes allowed transmittance of the NIR, ultraviolet (UV), and excimer beams. Pre-cooled gasses flowed into the cell

through an off-center entrance port and then out of the cell at two exit ports on either side of the cell. The total path length between the centers of the exit ports was 138 cm. Room temperature nitrogen purge gas entered the experiment through each mirror housing box as well (not illustrated above). This purge gas met the reactant gas at the exit ports to confine the reactant gas to the temperature controlled region. The total path length from the window of one mirror box to the window of the other was 208 cm. All flows were monitored using mass flow meters (Hasting HFM-200 series). The volume of the reactant flow region of the cell was ~2900 cm^3. Total flow velocities were calculated to determine the residence time of gas in the cell, i.e., the amount of time elapsed before an entirely new fill of gas occupied the cell. Residence times were typically on the order of 10 s. At a second off center port a Type T thermocouple (Omega) was threaded into the cell to measure the temperature, and a capacitance manometer (MKS-220CA 1000 Torr) was connected to measure pressure. Similar capacitance manometers were used to measure the pressure inside of the bubblers that brought vapor from liquid reagents to the flow cell.

A XeCl excimer laser (308 nm, ~ 100 mJ/pulse) was the photolysis laser, and made one pass through the cell. The laser pulse was recorded by a photodiode in order to signal the data acquisition program that a successful run had occurred. The laser generally operated at a repetition rate which allowed for one whole gas residence time to pass before firing again, e.g., for a residence time of 10 s the excimer operated at 0.1 Hz. Light from a 150 W deuterium (D_2) lamp (Hamammatsu L1314) also made one pass through the cell co-aligned but counter-propagating with the excimer beam. Dichroic mirrors were used to reflect the 308 nm excimer, but allow the deuterium light < 300 nm

to pass. NIR light from a distributed feedback diode laser passed through the cell 30 times reflecting back and forth off of two spherical gold mirrors in a Herriott cell configuration. These mirrors were placed slightly off the axis of the photolysis laser to allow the photolysis pulse to pass above and below the mirrors, respectively.

The diode laser was wavelength modulated (WM) to reduce the amount of noise in the absorption signal. A diagram and description of the WM set up and detection electronics are given in Section 5.5.1.

The data acquisition was controlled by a visual BASIC program. Pressures, flows, and the excimer firing signal were recorded with a NIDAQ data acquisition card (National Instruments CB68LP). The data signals from the NIR and UV probes were digitized using a two-channel 16 bit per channel A/D card with a maximum sampling rate of 2.5 MS/s (Gage-CompuScope 1602). The data was low pass filtered (SR560) before collection, and the filter setting was determined by the sampling rate. The Nyquist theorem dictates that signals at frequencies greater than one half the sampling rate will lead to aliasing, so for a typical sampling rate of 200 kSa/s the low pass filter was set to 100 kHz.

5.2 Absorption measurements

The goal of the IRKS apparatus is to measure kinetics and thermodynamics for a variety of peroxy radical (RO_2) chemistry. Experiments are put on an absolute scale by the concentrations determined from absorption in the UV. Beer's law shown in equation (5.1), relates the absorbance, *A*, to the concentration, [Conc] (molecules cm^{-3}), of the absorbing species through a proportionality constant made up of the product of the path length *l* (cm) and the absorption cross section σ (cm^2 $molecule^{-1}$).

$$A = [\text{Conc}] * l * \sigma \quad (5.1)$$

Absorbance measurements were performed for a variety of reasons including verifying methanol (CH_3OH) concentrations, verifying the reactant flow path length, measuring absorption cross sections, and verifying acetone concentrations. Work done in collaboration with graduate student Aileen Hui and Professor Fred Grieman also indirectly probed the path length by measuring the temperature profile along the length of the apparatus. Path length and absorption cross section measurements were necessary because both values are central to measuring absolute concentrations and absolute kinetics with the apparatus.

5.2.1 Experimental setup and verification

The initial absorption measurements were done with penray lamps (Hg at 185 nm and Zn at 214 nm). The setups for both penray experiment are shown in **Figure 5-2**. The flow cell was set up the same as it was for kinetics experiments, but the optics for the excimer laser, D_2 lamp, and diode laser were all removed to allow positioning of the penray lamp and photomultiplier tube (PMT) detector. A different PMT with a different photocathode was used depending on the penray lamp; a Cs-I photocathode was used for the Hg penray and a bialkali photocathode was used for the Zn penray. To obtain sufficient signal the Zn setup also required using 6 and 5 cm focal length optics at the entrance and exit of the cell, respectively. A picoammeter was used to read out the signals in both setups.

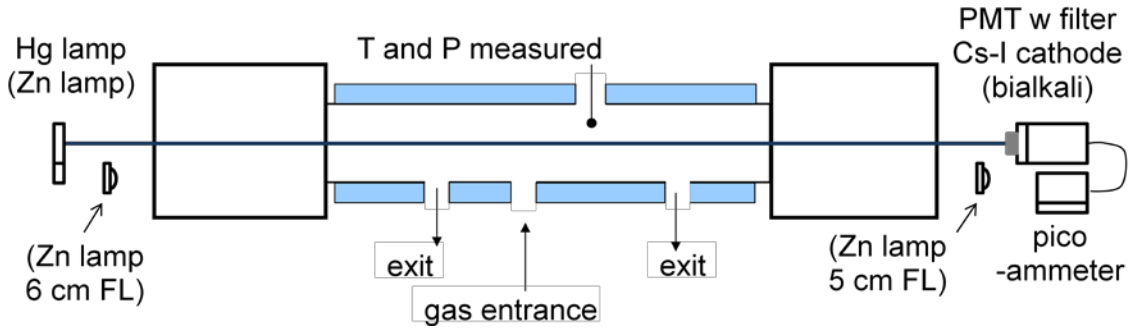

Figure 5-2. Setup for penray lamp experiments. To look at the 185 nm line from the Hg lamp a Cs-I photocathode PMT was used to reduce all light at λ > 190 nm. For the 214 nm line from the Zn lamp it was necessary to use focusing optics before and after the cell with a bialkali photocathode PMT. For both lamps a filter was used at λ = 185 or 214 nm to attenuate other wavelengths.

Absorption experiments were also done using the D_2 lamp as the light source, and were setup exactly as the normal kinetics experiments were in **Figure 5-1**. In a few cases a Cary UV-Vis spectrometer was used to verify absorption cross sections. A list of all the molecules that were studied including the method and λ that they were studied at is given in **Table 5-1**.

Table 5-1. Summary of all the molecules and λ where absorption measurements were made.

Molecule	λ (nm)	source	$\sigma_{full\ cell}$ / (cm^2)	σ_{lit} / (cm^2)	Path Length (cm) (100 Torr, 10 s res , 100% purge)
CH_3OH	185	Hg penray		6.30×10^{-19} [b]	
N_2O	214	Zn penray	3.35×10^{-21}	3.60×10^{-21} [b]	
N_2O	214	Cary	3.37×10^{-21} [a]		
N_2O	185	Hg penray	1.27×10^{-19}	1.40×10^{-19} [c]	
N_2O	185	Cary	1.36×10^{-19} [a]		
CF_3Br	185	Hg penray	4.23×10^{-20}	4.45×10^{-20} [c]	
CF_3Br	185	Cary	4.44×10^{-20} [a]		
CF_3Br	220	D_2 lamp	7.45×10^{-20}	7.56×10^{-20} [c]	149
Cl_2	295	D_2 lamp	8.52×10^{-20}	8.85×10^{-20} [c]	149
Acetone	275	D_2 lamp	4.96×10^{-20}	4.96×10^{-20} [b]	161

[a]Measurements were made in a 10 cm cell in the Cary spectrometer, [b] MPI-Mainz UV database,[3] [c] JPL-06 recommendation[4]

Absorption measurements were first attempted to verify the [CH_3OH] in the flow cell. The 185 nm line of the Hg penray lamp was used as a light source because of the suitable absorption cross section of CH_3OH at this wavelength. Measurements of N_2O at 185 and 214 nm, and CF_3Br at 185 nm followed in order to check the experimental setup. CH_3OH was introduced into the cell by bubbling N_2 through liquid CH_3OH held at 0 °C (V.P. 30 Torr)[5] and monitoring the total pressure in the bubbler. The N_2O and CF_3Br were supplied directly from gas cylinders. Nitrogen calibrated flow meters were used to monitor the flows of all gases by using the appropriate correction factors (0.75 for N_2O and 0.37 for CF_3Br) where necessary. The concentrations of each species in molecules cm^{-3} were: [CH_3OH] = $5 \times 10^{14} - 1 \times 10^{16}$, [$N_2O$] (185 nm) = $9 \times 10^{15} - 1.8 \times 10^{17}$, [$N_2O$] (214 nm) = $3 \times 10^{17} - 2 \times 10^{18}$, and [$CF_3Br$] = $3 \times 10^{16} - 3 \times 10^{17}$. The high voltage supplied to the PMTs was typically between 600 and 900 V.

Measurements were performed by measuring the intensity of light coming through the cell without any of the absorbing gas present, and then by measuring the light with a series of 4 – 5 different concentrations of the absorber present. A check of the baseline intensity was performed after evacuating the cell, and the measurements repeated. Fluctuations in the measured signal were a common problem. The estimated precision of the signal measurements from the picoammeter due to these fluctuations was ± 0.005 μA.

The first attempts at penray measurements using the 185 nm Hg line failed because of light from both 254 and 194 nm lines leaking through the single 185 nm filter being used. Good measurements were made by either using two 185 nm filters (Acton 185-HR-1D-MTD) or one filter and a PMT with a Cs-I photocathode. A Cs-I

photocathode attenuates light at $\lambda > 190$ nm, and was used in penray measurements done by Cantrell et al. and Creasey et al on N_2O absorption.[6,7] **Figure 5-3** shows the absorbance plots for N_2O at 185 nm with the bialkali and Cs-I PMTs. The curvature was obvious in the bialkali case.

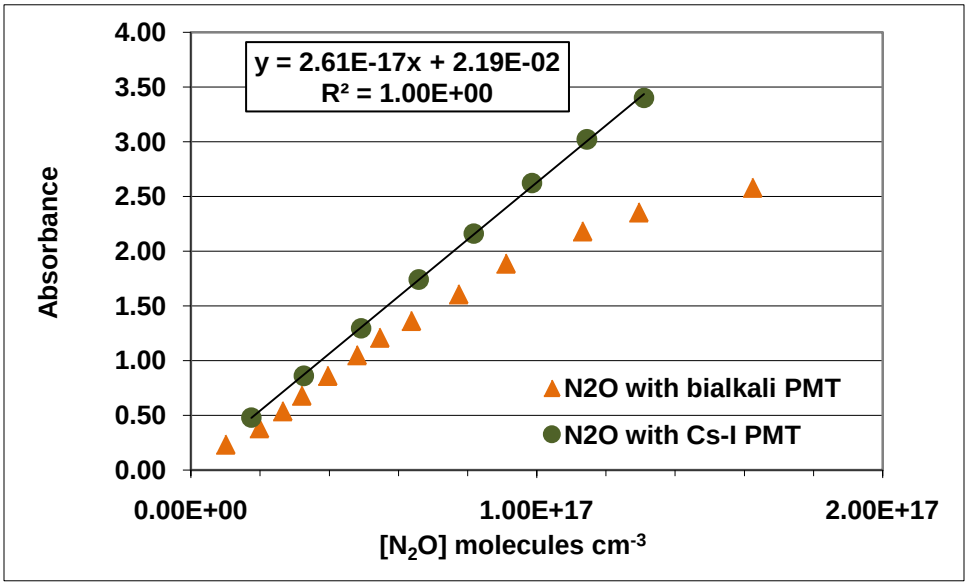

Figure 5-3. Curvature in the absorbance plot for N_2O was seen when using the PMT with the bialkali photocathode, but not when using the Cs-I photocathode.

Static cell and Cary spectrometer measurements of the absorption cross sections for N_2O and CF_3Br were made to verify the values from the literature. The static cell measurements used the 208 cm path length that was fixed by the window – window distance of the kinetics cell. Each gas was allowed to fill the cell, and the total concentration was determined from the pressure in the cell by using the ideal gas law. For the Cary measurements a 10.5 cm cell with NaCl windows was attached to the main kinetics cell to fill, and then was taken to the Cary. For each concentration 15 s averages were recorded 10 times and then those 10 recordings were averaged. The spectral bandwidth was 0.5 nm. Some clear nonlinearity could be observed in the Cary absorbances, but these could be fit with equation (5.2) to give good cross section values.

$$I_t = I_0\left(e^{-(\sigma * l * c)} + \mathrm{E}\right) \quad (5.2)$$

E is the error term associated with the nonlinearity and was usually around 0.05. All of the measured cross sections and their literature values are shown in **Table 5-1**. Good agreement was seen between the CF_3Br and N_2O cross sections measured and their literature values, verifying the overall absorption measurements.

5.2.2 [CH_3OH] measurements

Using the procedure for the 185 nm absorption measurements established with N_2O and CF_3Br, measurements of [CH_3OH] were made under normal flowing conditions for the kinetics flow cell. Concentrations of CH_3OH measured by absorption agreed with the concentrations calculated from the flows when the total pressure in the CH_3OH bubbler was kept above 300 Torr. At pressures < 300 Torr, [CH_3OH] measured was larger than the calculated value. The 300 Torr mark was true for a variety of temperatures as can be seen in **Figure 5-4**. At 222 K, the lowest temperature on the plot, the absorption measurements became nonlinear at 1 x 10^{16} molecules cm^{-3}. This was also true at 210 K at ~ 1 x 10^{15} molecules cm^{-3}. Condensation or dimer formation of CH_3OH was probably occurring, making these conditions approximate limits of temperature and CH_3OH for this experiment.

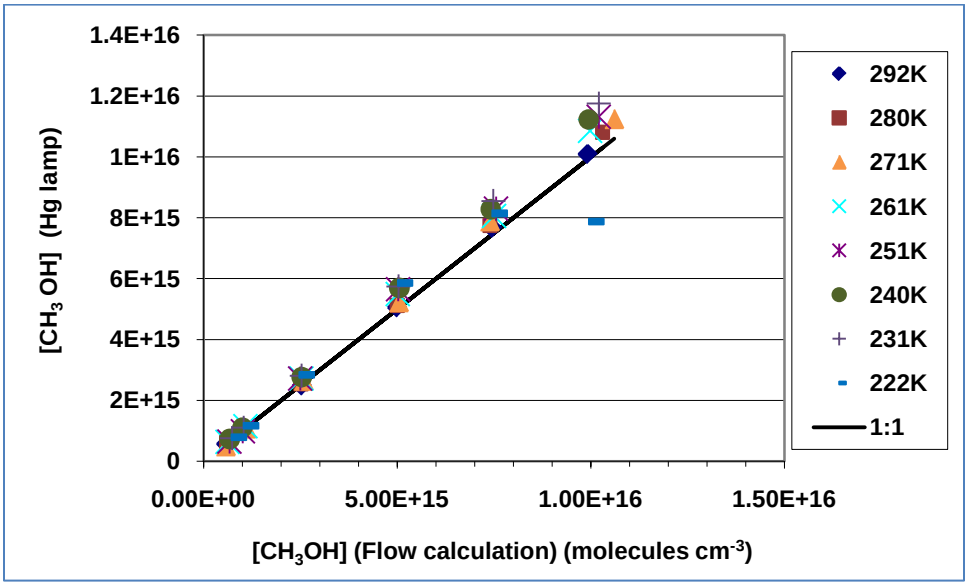

Figure 5-4. [CH_3OH] measured by the Hg lamp agrees with the concentration determined by the flows when the bubbler pressure is above 300 Torr.

The measured values were still slightly larger than the predicted ones. This data was analyzed with a path length of 138 cm, however most of the data fit even better using a path length between 145 and 155 cm. This is in agreement with the path length data discussed next, and is consistent with the current understanding of the flow system.

5.2.3 Path length measurements: Cl_2 and CF_3Br

After observing some counterintuitive kinetics results it was necessary to investigate the reactant path length and how it was affected by pressure, residence time, and the amount of purge flow as a percentage of the total reactant flow. Both Cl_2 and CF_3Br were investigated using the D_2 lamp as a light source so that the absorption measurements could be made in the same optical configuration as the kinetics measurements. Static cell measurements were performed to check the Cl_2 and CF_3Br cross section at 295 and 220 nm, respectively; **Table 5-1** displays the good agreement in those values. Cl_2 measurements were important because Cl_2 was the radical precursor in the kinetics experiments so it was a direct proxy for the radical path length. Agreement

between the measured path lengths of Cl_2 and CF_3Br allowed most of the measurements to be carried out with CF_3Br, a safer gas to work with. All of the measurements made with CF_3Br at different flow conditions are shown in **Table 5-2**.

Table 5-2. Path length measurements at different residence times, pressures, and amount of purge flow as a percentage of the total reactant flow.

Residence Time (s)	P (Torr) / % purge	50	100	200	400
5	10	156.1	150.8		
5	25	150.8	149.5		
5	50	152.1	149.5		
5	100	150.8			
10	10	152.1	154.8		
10	25	152.1	150.8	*153.4	
10	50	150.8	146.8	*150.8	
10	100	148.1	144.2	*145.5	
15	10	161.4	162.7		
15	25	157.4	156.1	153.4	
15	50	154.8	152.1	149.5	
15	100	149.5	148.1	144.2	
20	15				165.3
20	50				150.8

*Purge flows are not exactly as stated. High pressure and short residence times required flows too large for the system.

The measured path lengths vary over 144 – 165 cm. A number of trends were observed both from the table and from the absorbance plots. The longer the residence time the more important the purge flow became in confining the reactant flow. The same trend was observed for increasing pressure, but it was less dramatic. To place the previous [CH_3OH] measurements in context, they were taken at 100 Torr, 5 s residence time, and 15% purge. From the table they should have shown a path length of ~ 150 cm, in agreement with what was noted as providing the best fit to the data. From **Table 5-2** the best condition for confining the reactant flow to the 138 cm exit port distance was 100

Torr total pressure, 10 s residence time and 100 % purge. These conditions were adopted as the ones to use for kinetics experiments.

5.2.4 Path length measurements: Acetone

A different path length was measured for acetone than for Cl_2 and CF_3Br. These measurements were made during collaboration with Professor Fred Grieman on work investigating the reaction of HO_2 with acetone. Acetone was introduced to the cell in a manner similar to the CH_3OH. A glass bubbler filled with liquid acetone was held at constant temperature and nitrogen gas was bubbled through at a known total pressure. Acetone concentrations ranged from ~ $5 \times 10^{15} - 2 \times 10^{16}$ molecules cm^{-3}. Initial measurements were done to double check the Cl_2 and CF_3Br cross sections using the D_2 lamp in the kinetics setup. Then the acetone cross section at 275 nm was measured in a flowing experiment (not a static experiment), but purge gas was not used so that the reactant flow filled the entire cell path length. Concentration was calculated from the flows and pressures, a method that was previously validated in the CH_3OH measurements. Static cell measurements were not done because of concern that the acetone might stick to the walls of the cell. Concentrations were allowed to stabilize for a few minutes each time the flow was changed during these measurements. **Table 5-1** shows the cross section for acetone and its agreement with the literature value. This further validated the bubbler method for acetone as well as the flow system calculations of concentrations. Path length measurements using acetone were then made under the flowing conditions of choice, i.e., 100 Torr, 10 s residence time, and 100% purge. These measurements consistently saw a path length of 162 cm, ~ 10 cm longer than what the Cl_2 and CF_3Br measured under identical conditions. This path length was consistent over

the temperature range 229 – 296 K. No obvious explanation for the path length difference could be found until the next experiments, that used temperature measurements as path length proxies, were able to provide one.

5.2.5 Path length measurements: Temperature probe

The current understanding of the path length was determined by work performed with Aileen Hui and Professor Fred Grieman to measure the temperature profile of the gas along the length of the flow cell. A thermocouple probe was attached to the end of a movable steel rod and a temperature was taken at each point as it was moved throughout the cell. Purge gas flow was at room temperature and the reactant gas flow was at 213 K. By measuring where in the cell the temperature gradient from 296 to 213 occurred it was possible to determine both the length and the absolute location of the mixing between the purge and reactant flows. Under the conditions of 100 Torr, 10 s residence time and 100 % purge, the total path length including the entire mixing region on both sides was ~ 160 cm. The path length connecting the midpoints of the mixing region was ~ 150 cm.

An explanation for the path length difference between acetone and Cl_2/CF_3Br was provided by the difference in the “total” and “midpoint” lengths. A sticky molecule like acetone that can build up concentration on the walls of the cell as a reservoir will have a path length along the whole range of the mixing region even if the initial gas phase amount is diluted. Molecules such as Cl_2 and CF_3Br that do not interact with the walls will appear to have a length that stretches from the midpoint of one mixing region to the other because the more dilute portions of the mixing region do not contribute significantly to the measured path length.

Another measurement was made at 300 Torr that showed the same qualitative behavior, but this time the total length had reached ~ 170 cm and the size of the mixing regions was larger than at 100 Torr. This confirmed doubts about higher pressure kinetics measurements that had been made on HO_2 and RO_2 self reactions (Discussed next in section 0), suggesting that the data was probably unreliable due to the large mixing regions where concentration gradients would lead to different reaction rates occurring. In general the temperature probe measurements provided a much better understanding of the purge and reactant gas dynamics, as well as the measured reactant flow path lengths.

The probe measurements also revealed a temperature offset in some of the data due to misplacement of the fixed thermocouple in the cell. Within a small radius of the port that allowed for the thermocouple and capacitance manometer to be attached to the cell the temperature was higher due to the lack of coolant flowing in that region. When the thermocouple was threaded further down the cell it then agreed with the temperature probe. A calibration was determined and was applied to the data affected during the nucleation experiments described in Chapter 4.

5.3 Pressure dependence of the HO_2 and RO_2 self reactions

One of the motivating factors for more carefully determining the path length was to investigate the pressure dependence of HO_2 and RO_2 self reactions. Initial studies with this system did not observe a pressure dependence for the HO_2 self reaction and actually saw an inverse pressured dependence for the $C_2H_5O_2$ self reaction when looking at data taken with the D_2 lamp (UV) probe. The HO_2 self reaction has a reported pressure dependence, and $C_2H_5O_2$ has been measured as having no pressure dependence so something appeared wrong with the measurements.[4]

The procedure for studying the pressure dependence was to set the bulk flows and pressure at one value, then adjust the Cl_2 concentration from ~ 3 x10^{15} – 1.5 x 10^{16} leading to initial RO_2 concentrations of ~ 3 x 10^{13} – 1.5 x 10^{14} molecules cm^{-3}. The data was analyzed over a variety of different time scales, but the procedure that was settled on was to analyze all the data over a consistent number of half lives for every concentration. Frequently 2 half lives were used, but when possible 3 half lives were used as well.

5.3.1 HO_2 + HO_2

From the data shown in **Figure 5-5** what immediately stood out was the dependence of the UV rate constant for the HO_2 self reaction, $k_{HO2}(UV)$, on initial radical concentration.

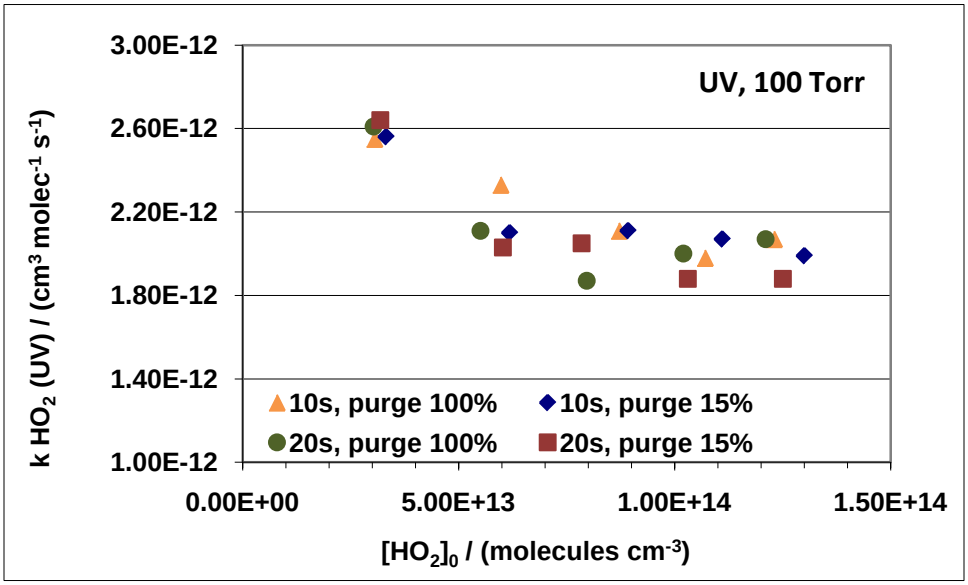

Figure 5-5. Initial radical dependence of the HO_2 self reaction observed by the UV. Concentrations < 5 x 10^{13} were influenced by other removal processes.

At concentrations < 5 x 10^{13} molecules cm^{-3} the $k_{HO2}(UV)$ increased for all of the flow conditions shown indicating that another removal process was important. This was not observed in **Figure 5-6** for $k_{HO2}(NIR)$.

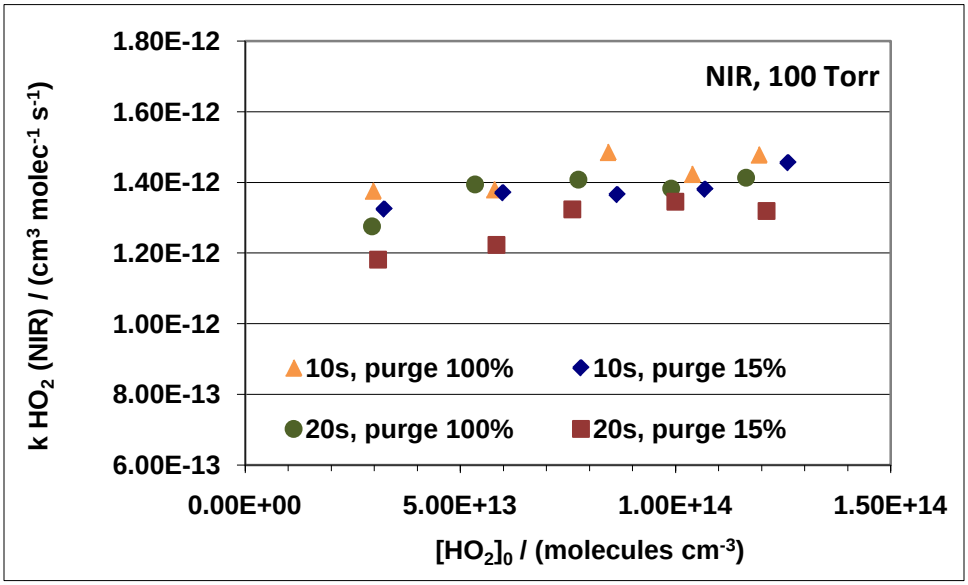

Figure 5-6. Initial radical dependence of the HO_2 self reaction observed by the NIR.

At much lower radical concentrations this was eventually seen in the NIR as well, but at those concentrations the UV signal-to-noise was very low so comparison was difficult. The pressure dependence of both $k_{HO2}(UV)$ and $k_{HO2}(NIR)$ are shown in **Figure 5-7**. The data were taken using the flow conditions determined by the absorption measurements to best contain the reactant flow in **Table 5-2**. The NIR behavior was not always consistent, but did show a dependence on pressure while the UV was consistently independent of pressure.

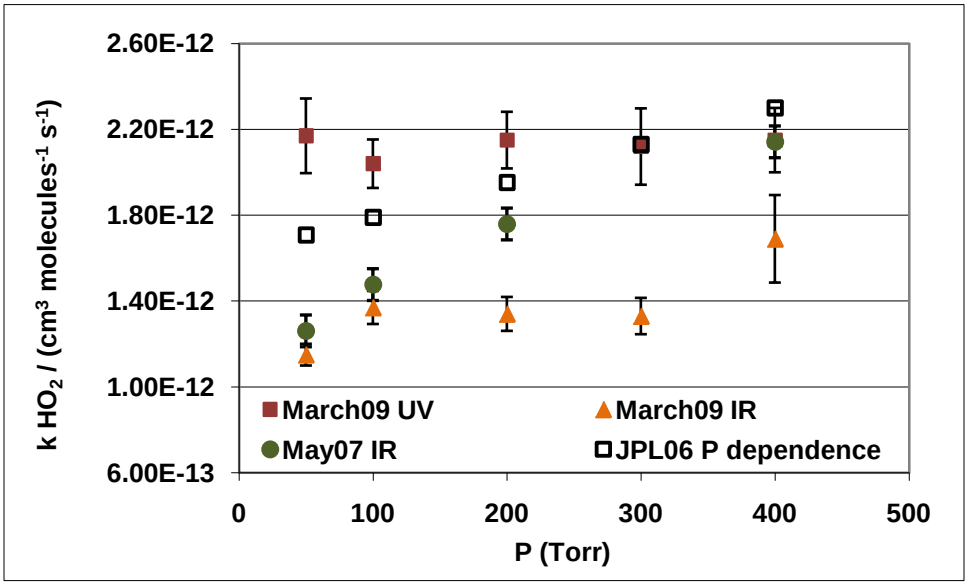

Figure 5-7. Pressure dependence of k_{HO2} in both the UV and NIR compared with the literature value. The NIR behaved differently at different times.

The lack of pressure dependence in the UV prompted further UV experiments that were done completely without purge gas. Similar to the flowing absorption cross section measurements of acetone, path length was physically fixed by the window – window distance of the reaction cell. These results, shown in **Figure 5-8**, did show pressure dependence. They also show a similar initial radical dependence to the 100 Torr measurements of $k_{HO2}(UV)$.

The UV setup was very straightforward due to the coalignment of the D_2 beam with the excimer laser. At first thought any deviations in the pressure dependence and behavior with radical concentration would be expected in the NIR, where the off-axis overlap could lead to more complicated behavior. By comparing the results in **Figure 5-7** and **Figure 5-8** it is clear that the presence of the purge flow must be what eliminated the observed pressured dependence. Without a purge the $k_{HO2}(UV)$ agrees very well with the literature. The comparison also shows that the behavior of $k_{HO2}(UV)$ at low radical is not related to the purge because it is present in both figures. One explanation is that removal

by diffusion out of the D_2/excimer beam path is also a significant loss process at concentration < 5 x 10^{13} molecules cm^{-3}, but this will be discussed further in Section 5.3.2.

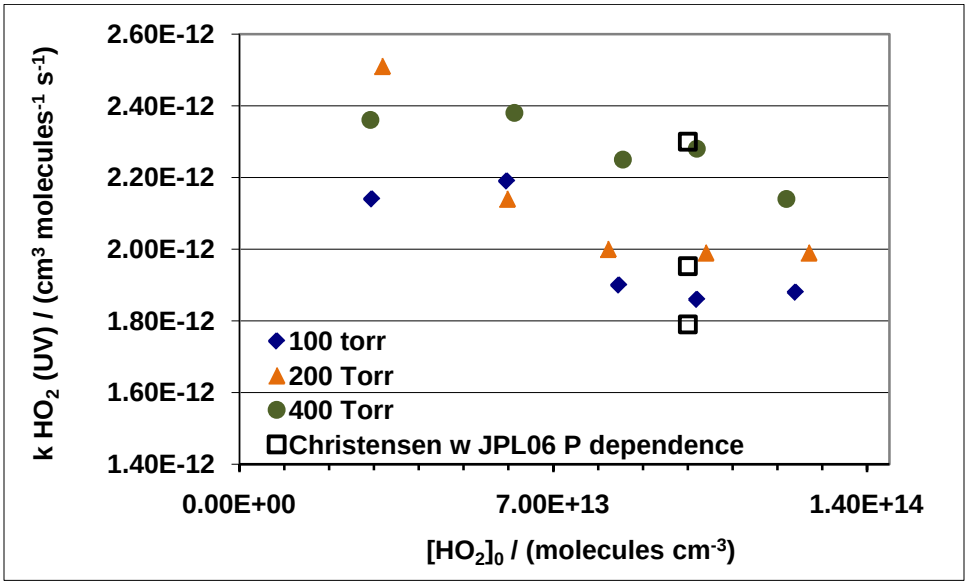

Figure 5-8. Pressure dependence of $k_{HO2}(UV)$ under conditions where no purge gas was used and the path length was fixed by the window – window distance.

Another issue was that the $k_{HO2}(UV)$ and $k_{HO2}(NIR)$ values at 100 Torr were different. The $k_{HO2}(UV)$ was somewhat high as shown because it was analyzed with the absorption path length determined from the CF_3Br etc. absorption measurements described above, i.e., 148 cm. However it may be that a "kinetics" path length was more appropriate for the analysis of the data. The kinetics path length was determined by fixing $k_{HO2}(UV)$ to the value measured in the non-purge case (where path length was known), and then fitting the path length. Path lengths determined in this way for the 100 Torr data were equal to ~ 138 cm. In these fits path length and $k_{HO2}(UV)$ are proportional so lowering one will lower the other. The kinetics path length agrees with measurements from the thesis of Dr. Christensen, which also used absorption measurements, but primarily relied on a kinetics determination to come up with a path length of 138 cm.[1]

Given the uncertain nature of the path length from the temperature probe observations, a kinetic path length may best measure the effective path length of the chemistry.

The low value of $k_{HO2}(NIR)$ was harder to explain and appeared to come from the off axis geometry of the NIR beam overlap with the radicals produced in the excimer laser. The off axis alignment means that as diffusion causes some molecules to leave the NIR beam path in the center it causes others to enter the beam path at the extremes where previously no radicals have been. This leads to an elongated path length at longer times and artificially higher signal at these times, i.e., it appears to slow the reaction down. To some extent it was sensitive to the alignment of the two lasers, as can be seen from the two different sets of pressure-dependent data. As expected it was not sensitive to the purge flow, unlike the UV, because the main overlap of the NIR laser with the excimer beam was in the center of the cell away from the purge regions. Further implications of the $k_{HO2}(UV)$ and $k_{HO2}(NIR)$ are discussed in Section 5.3.3 when discussing the CH_3OH effect on the HO_2 self reaction.

The NIR geometry effect also explained the lack of an $[HO_2]_0$ dependence for $k_{HO2}(NIR)$ over the same concentration range where there was one observed for $k_{HO2}(UV)$. This was handled in the fitting of the data by including a unimolecular loss term for the UV signal but not the IR. At the higher radical concentrations generally used for kinetics experiments this term had a negligible impact on fast reactions like the HO_2 self reaction, but was included for consistency. The determination of the unimolecular loss term is discussed next.

5.3.2 $RO_2 + RO_2$

RO_2 self reactions are considerably slower than the HO_2 self reaction and therefore more susceptible to interference from other loss processes. **Figure 5-9** shows the k_{obs} for the CH_3O_2 and $C_2H_5O_2$ self reactions plotted against the inverse of initial radical concentration. A clear linear dependence was observed unlike the $k_{HO2}(UV)$ data.

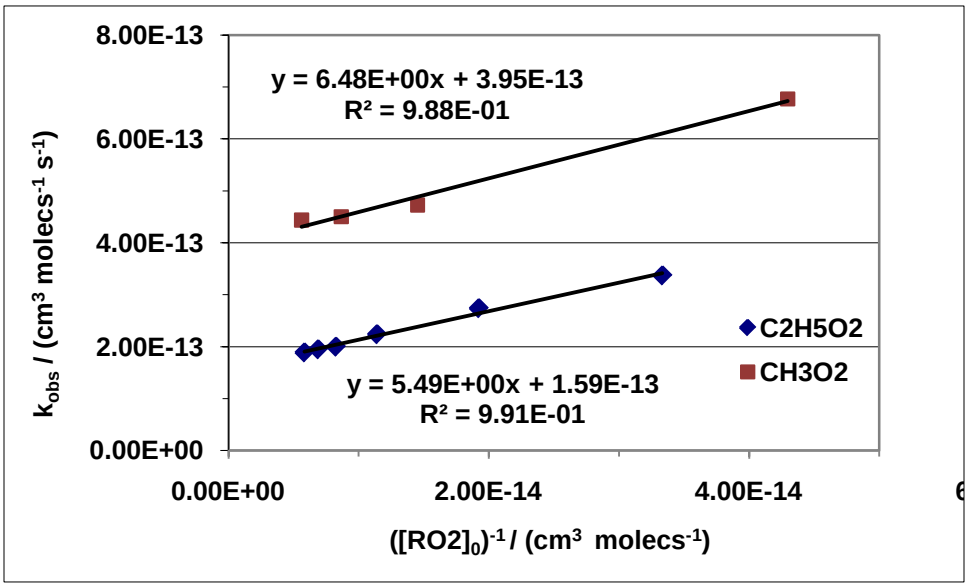

Figure 5-9. RO_2 self reaction dependence on initial radical concentration. A unimolecular diffusion loss was nonnegligible.

The initial radical dependence of the RO_2 self reactions was attributed to a larger impact from competing unimolecular loss, e.g., diffusion, because of the smaller k_{obs}. The effect of this loss was determined in two different ways. The kinetics of the RO_2 self reaction including a unimolecular loss term are described by equation (5.3).

$$\frac{d[\mathrm{RO_2}]}{dt} = -2k_{RO2}[\mathrm{RO_2}]^2 - k_D[\mathrm{RO_2}] \qquad (5.3)$$

This chemistry was modeled by the FACSIMILE program,[8] but needed a fixed value of k_D. The model could not successfully fit both k_{RO2} and k_D without either returning unphysical values or determining that the data was not dependent on k_D. The IGOR

software package was also used to fit the data using the analytical solution for bimolecular self reaction kinetics in equation (5.4).

$$\frac{1}{[\mathrm{RO_2}]_t} = \frac{1}{[\mathrm{RO_2}]_0} + 2k_{obs}t \tag{5.4}$$

The fits and residuals from the data looked good indicating that the analytical solution adequately described the time dependence of the concentrations. However k_{obs} was not consistent with initial radical showing that all losses were not being described. The fact that FACSIMILE could not determine a dependence of the data on k_D, the analytical solution fit well, but k_{obs} was inconsistent suggested that the unimolecular loss had a small but non-negligible effect on the reaction. By assuming that the effect is small, an analytical method for determining k_D was used, based off of the work from Thiebaud et al,[9] and shown in equation (5.5). Unimolecular loss is approximated without disturbing the analytical solution in equation (5.4), except that the expression in parenthesis of (5.5) is equal to k_{obs}.

$$\frac{d[\mathrm{RO_2}]}{dt} = -2\left(k_{RO2} + \frac{k_D}{[\mathrm{RO_2}]_0}\right)[\mathrm{RO_2}]^2 \tag{5.5}$$

Plotting k_{obs} vs. $([\mathrm{RO_2}]_0)^{-1}$ led to the linear fits seen in **Figure 5-9**, with k_D as the slope and k_{RO2} the intercept. FACSIMILE fits using the k_D from this method determined an identical k_{RO2} verifying the approximation of (5.5). The only exception was at some of the very lowest radical concentrations the points did not lay on the line. The low signal to noise in these cases made the data less reliable, and the increased importance of the diffusion loss meant the approximation in equation (5.5) was no longer valid.

The pressure dependence of the $C_2H_5O_2$ self reaction did not display the expected results. Similar to the HO_2 self reaction showing no pressure dependence when a positive

dependence was expected, this reaction showed a negative pressure dependence when no dependence was expected. Unlike the HO_2 self reaction removing the purge gas did not change things. **Figure 5-10** shows the pressure and initial radical dependence under both purge and full cell condition for the $C_2H_5O_2$ self reaction. It appeared from this that unimolecular loss was of larger importance than any purge effects. The 100 and 200 Torr k_{obs} led to similar k_{RO2}, but the 50 Torr k_{RO2} was larger. As discussed in Chapter 2, adjusting the k_D value to scale with pressure, (e.g., scale the measured 50 Torr k_D = 5 s^{-1}, to a 100 and 200 Torr k_D of 2.5 and 1.25 s^{-1}, respectively) led to better agreement.

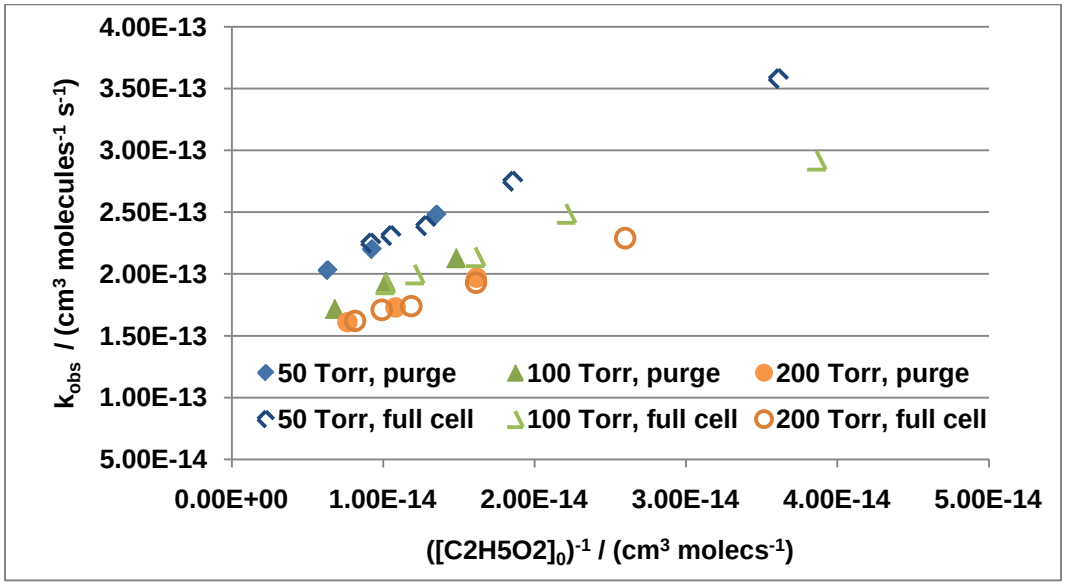

Figure 5-10. Pressure dependence of $C_2H_5O_2$ self reaction did not change with or without the purge gas.

The exact nature of the unimolecular loss, whether it is diffusion or due to a flow effect, is difficult to determine. In his thesis, Dr. Lance Christensen assigned the dominant loss to turbulent mixing as opposed to diffusion because of a dependence on the residence time of the flow.[1] In this work flow changes and faster residence times also appeared to be able to increase the apparent removal rate at both 100 and 200 Torr (but not their extrapolated k_{RO2} values), but further slowing of the flow did not change the 50

Torr data. One explanation is that there are flow effects that dominate at the higher pressures when diffusion is slower, hence the lack of reduction in measured k_D at higher pressure, but that at some point diffusion loss becomes comparable or greater than the flow loss at lower pressure. Pushing the upper limit of the radical concentration at higher pressure would show that it stops obeying equation (5.5), and reaches a constant value of k_{RO2} at a larger value than expected if the flow loss really is the culprit. Alternatively, the unimolecular loss may somehow be under predicted at 50 Torr leading to values of k_{RO2} that are too large, but as also previously mentioned in Chapter 2, increasing k_D above the values determined leads to worse fits to the data. Overall the combined unimolecular loss processes are well fit for the slower k_{RO2} measurements and have a negligible effect on the higher concentration k_{HO2} measurements.

5.3.3 HO_2 + HO_2 and the CH_3OH effect

The HO_2 self reaction was more complicated to study because of interference from the CH_3OH precursor chemistry. HO_2 was generated by the following reactions:

$$Cl_2 \xrightarrow{h\nu\ 308\ nm} 2Cl \tag{5.6}$$

$$Cl + CH_3OH \longrightarrow HCl + CH_2OH \tag{5.7}$$

$$CH_2OH + O_2 \longrightarrow HO_2 + HCHO \tag{5.8}$$

This chemistry worked very well because it generated only HO_2 and the stable products HCl and HCHO, except for one known problem, HO_2 and CH_3OH form a hydrogen bonded complex at low temperature. This complex increases the observed rate of the HO_2 self reaction and must be accounted for when trying to determine the actual rate coefficient of the self reaction for the atmosphere.[10-13]

$$HO_2 + HO_2 \xrightarrow{M} H_2O_2 + O_2 \quad (5.9)$$

$$HO_2 + CH_3OH \rightleftharpoons HO_2 - CH_3OH \quad (5.10)$$

$$HO_2 + HO_2 - CH_3OH \longrightarrow H_2O_2 + O_2 + CH_3OH \quad (5.11)$$

At higher concentrations of CH_3OH reaction of the complexes may occur or additional CH_3OH may complex with one HO_2, e.g., $HO_2 - (CH_3OH)_2$, as was discussed in Chapter 4 during the nucleation experiments.

The effect of the complex on the observed kinetics was also temperature dependent because the complex becomes much more heavily favored at low temperature. **Figure 5-11** shows the k_{HO2} values obtained while taking the data in for the $C_2H_5O_2$ system in Chapter 2. As just shown at room temperature the $k_{HO2}(UV)$ is a little bit larger than $k_{HO2}(NIR)$, but overall there was acceptable agreement until ~ 230 K. At low temperature $k_{HO2}(NIR)$ was much larger. In this regime the NIR and UV probes were starting to observe different overall kinetics due to the HO_2-CH_3OH complex. In the UV the complex absorption cross section is likely to be similar to the HO_2 absorption cross section because the absorption is a B←X transition of a non-bonding O atom electron not involved with the hydrogen bond of the complex. Therefore total HO_2 is seen in the UV. In the NIR the frequency of the O–H stretch overtone of the HO_2 will likely be shifted because the H atom helps form the complex, and would not be observed at the same wavelength as the uncomplexed HO_2. Total HO_2 is then not observed in the NIR. This could lead to a larger measured rate constant because the faster disappearance is wrongly attributed to the rate coefficient rather than the unseen additional concentration of radicals. The $k_{HO2}(UV)$ agree with the Christensen et al. values also measured by the UV

in the same apparatus.[12] A complete and thorough data set reinvestigating the CH_3OH dependence of $k_{HO2}(UV)$ has not been completed, but after resolving the issue with the CH_3OH bubbler pressure and applying the temperature correction from the temperature probe experiments, the most recent $k_{HO2}(UV)$ CH_3OH dependence and zero CH_3OH values taken with Professor Fred Grieman were in agreement with the Christensen values.

One problem with the hypothesis that the NIR and UV are different because of the complex is the relatively small amount of complex predicted for the CH_3OH concentrations and temperatures in the values for **Figure 5-11**. Using the K_{eq} from the Christensen et al. work,[11] the amount of HO_2 in complex form from starting values of $[HO_2]_0 = 1.0 \times 10^{14}$ and $[CH_3OH] = 1.0 \times 10^{15}$ at 231 K, is ~ 5%. This seems like too small an amount to cause the divergence in $k_{HO2}(UV)$ and $k_{HO2}(NIR)$ observed.

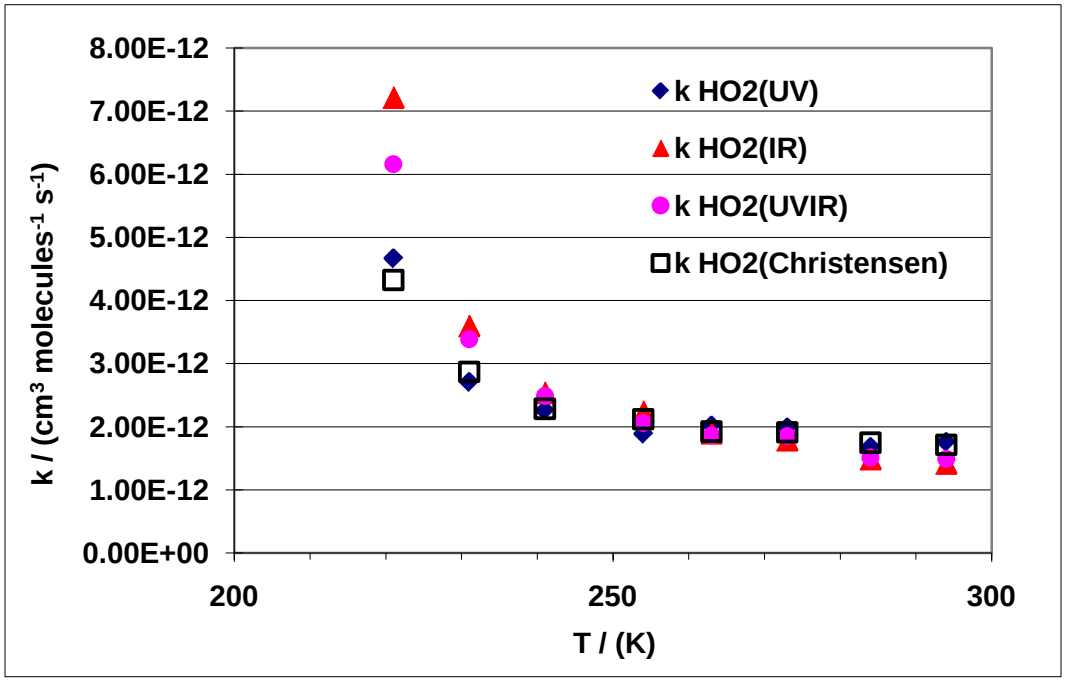

Figure 5-11. A comparison of the different k_{HO2} values from the work in Chapter 2 depending on whether the UV, IR, or UV and IR together were fit.

Work from other labs has measured a larger dependence on temperature for k_{HO2} actual than was measured by Christensen et al. in this lab.[12-14] A careful examination of the $k_{HO2}(NIR)$ would be interesting because of the stronger dependence on temperature just described. Purge flow might contribute to the differences between the NIR and UV because as also discussed the purge does not affect $k_{HO2}(NIR)$, but does affect $k_{HO2}(UV)$. The purge interference could be especially problematic at low temperature where the gas mixing regions will react more slowly because they are at higher temperature, thus potentially causing $k_{HO2}(UV)$ to appear lower than it actually is.

A simulation to test for a purge influence on $k_{HO2}(UV)$ was attempted based on the mixing profile measured using the temperature probe. The simulation was done in the following way: First, linear mixing of the room temperature purge (296 K) and the cold reactant gas (213K) was assumed to be responsible for the temperatures measured in the mixing region. The amount of each flow was assumed proportional to the temperature mixing, i.e., $T_{meas} = T_{room}*X + T_{cell}*(1-X)$, where X is the fraction of purge in the mixture. Using these fractions and a typical HO_2 initial of 7×10^{13} molecules cm^{-3} in the pure reactant flow, the appropriate fractional-initial concentrations in the mixing regions were determined. A FACSIMILE simulation of the HO_2 self reaction at each initial concentration was then run. Each of these simulations (HO_2 time profiles) was then multiplied by the HO_2 cross section and the path length over which that fraction exists to come up with an absorbance. The path length was determined by the spacing between temperature measurements, so it was somewhat arbitrary. However in the mixing regions measurements were generally made every 1–2 cm leading to a reasonably fine grid within the rapidly changing region. A similar procedure was followed for the H_2O_2 product and

was added into each absorbance. All the absorbances for the entire cell path length were then added together to form a simulated HO_2 absorbance trace, and then fit using the standard model like conventional data. This was done for 100 Torr and 300 Torr at room temperature and 100 Torr at 213 K. (In the 213 K case the only additional difference was that the rate coefficient at each fraction was also adjusted for the temperature at that fraction). The results are shown in **Table 5-3**. The simulations predict a clear lowering of the measured $k_{HO2}(UV)$ value at low temperature, and this value was not far from the value that would be extrapolated from the Christensen et al. measurements. On the other hand the simulation showed that although both 100 and 300 Torr would be lower than expected a clear pressured dependence would still exist. This was not observed in the actual experiment, leaving questions about the usefulness of the simulations given that they were not clearly validated by the measurements.

Table 5-3. Simulation of purge effect on $k_{HO2}(UV)$ at low temperature and high pressure.

T (K)	P (Torr)	CH_3OH (molecules cm^{-3})	$k_{HO2}(UV) / 10^{-12}$		
			Input	Output	Measured
298	100	2.00×10^{15}	1.78	1.57	1.70
298	300	2.00×10^{15}	2.09	1.83	1.80
213	100	2.00×10^{15}	3.48†	2.74	2.48*

* Extrapolated from the Christensen et al. value. †Taken from JPL06 recommendation.

In addition, the temperature dependent work for the $C_2H_5O_2 + HO_2$ reaction in Chapter 2 was in agreement with the literature, which suggests that the purge mixing might contribute only a small error to the overall kinetics. A final note on the $k_{HO2}(UV)$ and $k_{HO2}(NIR)$ comparison is that the $k_{HO2}(NIR)$ value was always dependent on the UV probe for it absolute calibration. This makes it difficult to totally separate the analysis when comparing trends. Two ways this might become relevant are through a greater than

expected temperature dependence of the HO_2 UV cross section, or a greater than expected shift in the HO_2–CH_3OH complex cross section. Both would affect the amount of $[HO_2]_0$ and the NIR calibration.

5.4 Summary of path length, pressure dependence, and CH_3OH effect

A number of experiments were carried out to better determine the effect of the flow conditions on the observed kinetics of HO_2 and RO_2 reactions. The calculated concentrations of the flow system have been verified by absorption measurements although the nature of the absorbing molecule (i.e., how sticky it is) will determine whether an absorption path length of 150 or 160 cm is correct for measuring concentration by absorbance. The most reliable flow conditions for containing the reactant flow were 100 Torr, 10 s residence time, and 100% purge. Cl_2 absorption (a good estimate of the true reactant path length because Cl_2 was the radical precursor) under these conditions had a path length of 150 cm, but kinetic determinations of the path length agreed with the 138 cm value determined previously. At this point an average of the two values, or simply the kinetics value, may be most appropriate.

The $k_{HO2}(UV)$ was also sensitive to purge and path length issues when examining the pressure dependence, but the unimolecular loss effects at low radical concentration occurred with or without purge. The disagreement between $k_{HO2}(UV)$ and $k_{HO2}(NIR)$ at low temperature may be accounted for by the spectroscopy of the HO_2-CH_3OH complex, but there may also be an effect due to the mixing region influencing the UV.

For the slower RO_2 self reaction k_{obs} was affected by unimolecular loss regardless of purge flow, but some residence time effects were also observed. The k_D measured did not show the expected dependence on pressure that a pure diffusion term would, leaving

some uncertainty in the cause of the loss. A unimolecular loss term that is a combination of diffusion and flow losses, the dominant loss depending on the regime of the flow, would describe the observed behavior.

5.5 NIR probe

The primary work of the IRKS apparatus has been kinetics measurements of RO_2 reactions by combining the sensitivity and specificity of the NIR probe with the absolute absorbance measurements of the UV probe. Spectroscopic measurements that took advantage of the sensitivity of the NIR probe were also possible. In this work the identification of molecular species and the optimization of the wavelength modulation (WM) signal were done by looking at the NIR spectroscopy. Other experimental noise issues in the NIR probe were also addressed.

5.5.1 NIR wavelength modulation setup

The NIR probe was a 1.5 μm distributed feedback diode laser made by the JPL microdevices laboratory. A 30 pass Herriott cell increased the path length of the NIR probe, shown schematically in **Figure 5-1**, and led to greater signal. WM spectroscopy was used to reduce the signal noise by allowing detection of the absorbance signal at higher frequency away from low frequency noise sources, and by measuring at a smaller overall bandwidth. The electronics of this system were setup by Dr. Lance Christensen and fully described in his thesis.[1] **Figure 5-12** shows the configuration of the electronics during the work of this thesis.

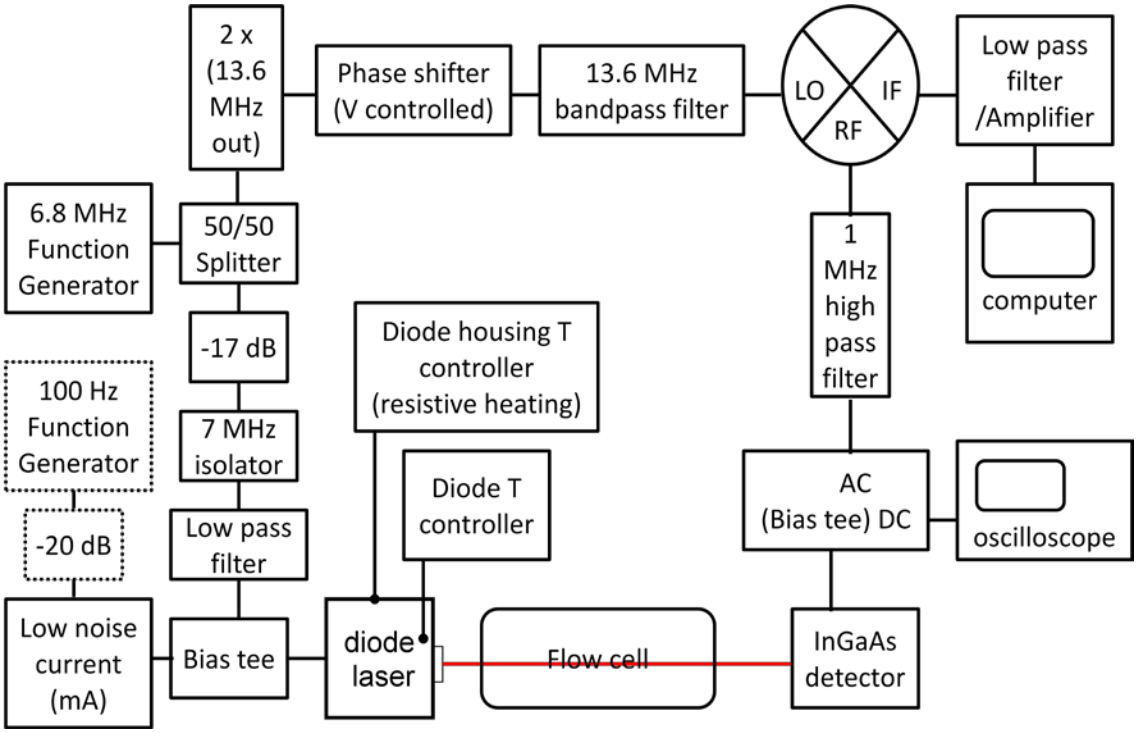

Figure 5-12. Diagram of the wavelength modulation setup for the NIR diode laser

The diode laser input current was modulated by at 6.8 MHz and the 2f signal was detected at 13.6 MHz. A 6.8 MHz, 10 Vpp, sine wave from a function generator (Agilent 33120A) was split (Mini-Circuits ZFSC-2-6), attenuated (Mini-circuits, various fixed attenuators), sent through a 7 MHz isolator (unknown manufacturer), and a low pass filter (Mini-Circuits SLP-5) before joining the DC current from the low noise current supply (ILX-Lightwave 3620) at a bias tee. The other half of the signal was doubled to 13.6 MHz (Mini-Circuits MK-3), phase shifted (Mini-Circuits SPH-16+) so that the signal at the mixer would be 90° out of phase with the original signal, and then sent through a 13.6 MHz bandpass filter (TTE KC4-13.6M) before ending at the LO of the mixer (Mini-Circuits ZFM-3+). Absorption in the flow cell converted the wavelength modulation of the diode laser to an amplitude modulation at the detector (New Focus 1811). A bias tee (Mini-Circuits PBTC-1GW) then removed the DC signal for monitoring on an

oscilloscope (Tektronix TDS 3054) and sent the AC signal to the mixer after passing through a high pass filter (TTE H93-1.0M). The output of the mixer was low pass filtered and amplified by a factor of 100 (SR560), and then the signal was sent to the computer. The low pass filter setting was determined by the data acquisition program and experimental conditions described in Section 5.1. For spectroscopy experiments a function generator (SRS DS340) was also used to ramp the current of the diode current source at 100 Hz, shown as dashed boxes in **Figure 5-12**.

5.5.2 HO_2 spectroscopy

Spectroscopy of HO_2 in the NIR has been looked at by a number of groups. Rovibrational lines in the A←X electronic transition have been investigated mainly in the 1.4 μm region.[15-18] The overtone of the O – H stretch ($2\nu_1$) was mapped out in work by Tuckett et al. and DeSain et al.[19,20] Line strengths in this region were also investigated by a number of groups primarily for use in kinetics studies.[9,11,21,22] The strongest transition observed so far is at 6638.2 cm^{-1}, the frequency used for detection of HO_2 in this apparatus. Frequency calibration of the NIR laser was done with a wavemeter borrowed from Dr. Pin Chen at JPL, and by comparison of the observed spectrum with a spectrum provided in a private communication by Dr. John DeSain at Sandia National Lab. **Figure 5-13** shows the observed HO_2 spectra as it changed in time at 6638.2 cm^{-1}, under the conditions $[HO_2]_0 \sim 9 \times 10^{13}$ molecules cm^{-3} and total pressure of 100 Torr. The data here has been divided by the background trace, shown in the figure as being taken in negative time. Without dividing the data by the background trace a sloping background was observed, partially due to the change in diode laser power with current. The background

also appeared to be somewhat dependent on the alignment of the Herriott cell because it changed from day to day.

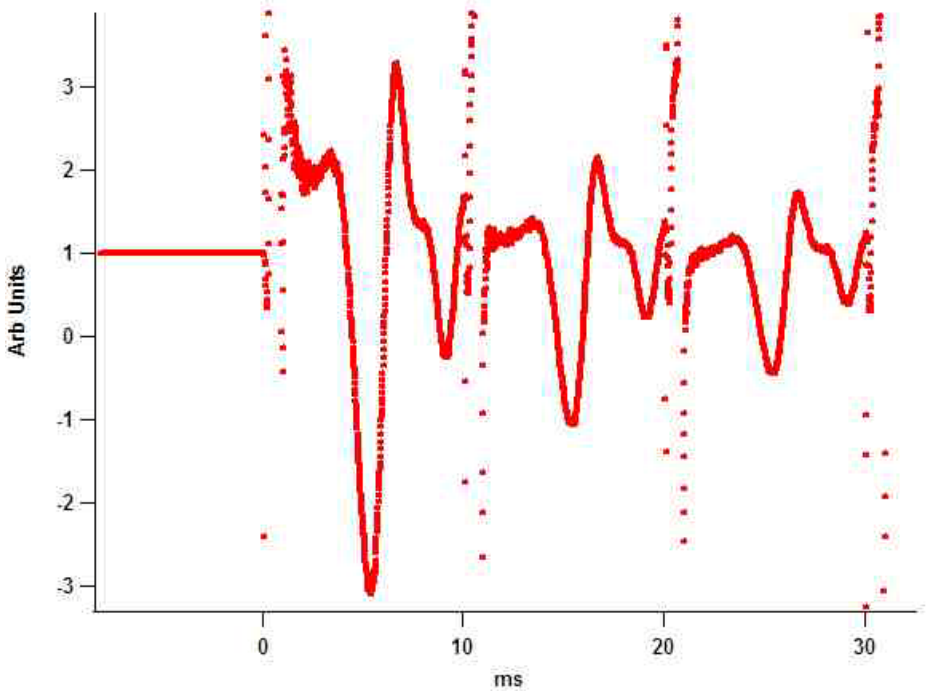

Figure 5-13. HO_2 spectrum after background ratio. The HO_2 self reaction reduces the signal as the scans are taken at progressively longer times after the excimer pulse. Two peaks are observed along with the characteristic 2f lineshape.

At certain alignments an etalon was the dominant source of noise in the spectroscopic experiments. In these cases adding a slight vibration (a foam damped personal foot massager was used as the vibration source) to one of the beam optics was found to reduce the noise from the etalon. A neutral density filter placed in front the detector to reduce the NIR beam power was also found to increase this etalon if placed perfectly perpendicular to the detector.

5.5.3 NH_3, CH_3CHO and C_2H_5OH

Spectra of ammonia (NH_3), acetaldehyde (CH_3CHO), and ethanol (C_2H_5OH) were all taken in the NIR as well. NH_3 came in pure form from a lecture bottle and its flows

were monitored using a mass flow controller. CH_3CHO/N_2 gas bulb mixtures were prepared on a vacuum line after freeze/pump/thaw purification of 95% pure CH_3CHO. The presence of pure CH_3CHO in the bulb was verified by using FTIR spectroscopy on a small sample from the bulb. Nitrogen bubbled through liquid C_2H_5OH held at 0 °C (V.P. 11.7 Torr) delivered C_2H_5OH to the cell. Concentrations in molecules cm^{-3} for each species were $[NH_3] = 1 \times 10^{14} – 4.5 \times 10^{16}$, $[CH_3CHO] = 1 \times 10^{14} – 3.0 \times 10^{16}$, and $[C_2H_5OH] = 3.5 \times 10^{15} – 3.5 \times 10^{16}$. In each case the laser current was scanned over ~ 15 mA which corresponded to ~ 0.75 cm^{-1}. Data acquisition was done directly with the digital oscilloscope since the excimer laser was not needed. Each scan was averaged 128 times.

The NH_3 work was undertaken as a frequency calibration. Strong lines were observed but the spectrum appeared congested and hard to interpret. Frequency calibration was then done using the wavemeter as already discussed. The confusing spectra were due to the fact that the modulation depth of the WM electronics was too large so individual transitions were being blended together. The modulation depth was corrected while observing the HO_2 spectra. No further work on NH_3 was done, but there are strong lines within the tuning of the diode laser bandwidth if needed in the future.

Measurements of CH_3CHO and C_2H_5OH were made to determine if either had an absorption that would interfere with HO_2 detection because both are products from the $C_2H_5O_2$ work in Chapter 2. No lines were observed within the tuning range even at concentrations as high as ~ 1 Torr.

5.5.4 NIR Baseline work

The NIR signal had an alignment-dependent baseline problem when following reactions for many milliseconds. Work investigating faster time scale processes such as the forward rate of the HO_2 – CH_3OH equilibrium constant was not affected by this, but longer time scale measurements of RO_2 self reactions were susceptible to interference. **Figure 5-14** shows this baseline problem for a HO_2 self reaction experiment. The dip was clearly related to the interaction of the excimer and diode laser beams as evidenced by the stable pre-photolysis baseline. Adjusting the Herriott cell alignment made it possible to achieve a stable baseline, but unfortunately no reproducible alignment procedure for removing the baseline was established.

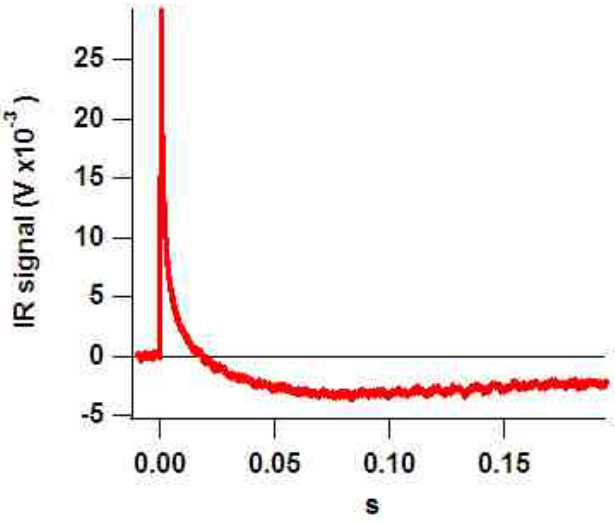

Figure 5-14. Baseline dip in HO_2 + HO_2 chemistry

An examination of the DC signal from the detector shows unequivocally the relationship between the NIR problems and the excimer laser. **Figure 5-15** shows two DC signals, one with only Cl_2 and O_2 and the other where ethane was also added to the mix. In both cases ringing in the signal can be observed, but it was even larger with ethane added. It appears that the exothermic initiation chemistry contributes to the coupling seen. This ringing could also sometimes be observed in the WM signal,

depending again on the alignment of the Herriott cell. The ringing occurred consistently at a frequency very close to 8 kHz. In fact this 8 kHz signal never completely disappeared, but with the correct alignment it was reduced to levels where other sources of noise dominated.

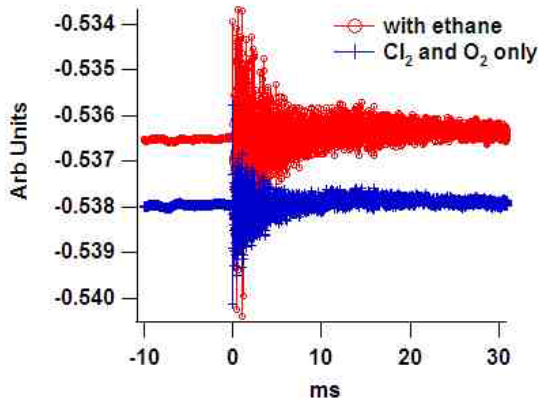

Figure 5-15. DC signal from the detector after the excimer fires. Energy released during the chemistry increases the noise, as can be seen by the larger noise when ethane was added to Cl_2 and O_2 mixtures.

When looking at the small secondary HO_2 signal from the $C_2H_5O_2$ self reaction it was critical that a stable baseline exist; it was unavoidable that the alignment always contained a bit of luck, but a straightforward diagnostic was possible. Because the source of the problem was the interaction of the excimer, the diode laser, and the chemistry it was likely that the dip was not wavelength dependent over the small tuning range of the laser. This allowed closer scrutiny of the baseline by tuning the laser off the HO_2 absorption line where no signal interference would occur. This was especially important because it allowed investigation of the baseline with the full chemistry in the cell which clearly led to larger noise in the DC signals of **Figure 5-15**. The "off HO_2 line" trace in **Figure 5-16** is an example of a good baseline signal that was measured by tuning the diode laser off the HO_2 absorption line. More traces at other wavelengths displayed similar baselines verifying the assumption that wavelength changes would not change the

baseline. Using this technique the criteria determined for a good alignment were that the baseline remain stable throughout the post photolysis time period, and that it not shift more than 500 μV.

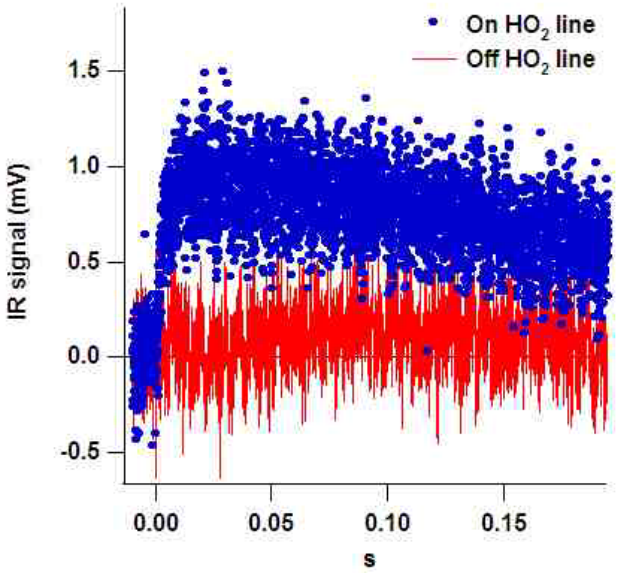

Figure 5-16. A signal is evident at the HO_2 frequency with only Cl_2 and O_2 present. A good baseline is also shown, determined by looking at its behavior while not on the HO_2 absorption line.

Also shown in **Figure 5-16** is the signal observed when only Cl_2 and O_2 are present in the cell and the laser is tuned to the HO_2 line. A real signal, not a baseline change, was observed. The species responsible was not known, but the signal was phase dependent indicating an actual absorption. This interference was initially mistaken for a baseline problem, and was another reason it was necessary to observe the baseline at a frequency other than the HO_2 line.

In general the quality of the WM signal was highly dependent on the alignment of the Herriott cell. The WM signal root mean square noise (RMS), the long time scale baseline, 8 kHz noise signal, and the stability of the DC signal all were sensitive to

optical alignment of the Herriott cell. With patience good quality signals in all categories simultaneously were possible.

5.6 Sensitivity of UV and NIR probes

The minimum detectable absorbance per $Hz^{1/2}$ (md*A* $Hz^{-1/2}$) for the UV and NIR probes allows comparison of the probes detection sensitivities. In the UV this was straightforward because absorbances are directly measured. The RMS noise of the UV absorbance signal taken with a 10 kHz bandwidth was ~ 2.8×10^{-3}. Using a signal to noise ratio (SNR) of 2 leads to md*A* $Hz^{-12} = 5.5 \times 10^{-5}$. The calculation in the NIR required a few approximations because the WM modulation signal was not an absolute absorbance. NIR signals were converted to concentration by a daily calibration in comparison to the absolute concentration measured by the UV. A simultaneous fit to the UV and IR time traces for the HO_2 self reaction chemistry allowed a voltage multiplier (VM) calibration factor to be established that converted the NIR signal in V to concentration in molecules cm^{-3}. The RMS noise of the NIR signal taken with a 10 kHz bandwidth was 2.47×10^{-4} V. Using a 100 Torr VM = 3.6×10^{14} molecules V^{-1} cm^{-3}, an estimated NIR path length of 2700 cm, and an estimated absorption cross section of 4×10^{-20} cm^2, the md*A* $Hz^{-1/2} = 1.9 \times 10^{-7}$ (Cross section and path length estimates come from Christensen et al.[2]). For day-to-day work with the apparatus the most straightforward diagnostic of the quality of the NIR signal was the VM. Due to pressure broadening of the line, sensitivity was almost directly proportional to pressure, i.e., a VM = 1.8×10^{14} molecules V^{-1} cm^{-3} at 50 Torr scales to VM = 3.6×10^{14} molecules V^{-1} cm^{-3} at 100 Torr. In general the signal in the NIR was good if VM • 4.0×10^{14} molecules V^{-1} cm^{-3} was measured at 100 Torr.

5.7 References

(1) Christensen, L. Laboratory studies of atmospherically important gas-phase peroxy radical reactions. , California Insitute of Technology, 2003.

(2) Christensen, L. E.; Okumura, M.; Sander, S. P.; Friedl, R. R.; Miller, C. E.; Sloan, J. J. *Journal of Physical Chemistry A* **2004**, *108*, 80.

(3) Keller-Rudek, H., Moortgat, Geert K. MPI-Mainz-UV-VIS Spectral Atlas of Gaseous Molecules, 2009.

(4) Sander, S. P.; Finlayson-Pitts, B. J.; Friedl, R. R.; Golden, D. M.; Huie, R. E.; Kolb, C. E.; Kurylo, M. J.; Molina, M. J.; Moortgat, G. K.; Orkin, V. L.; Ravishankara, A. R. "JPL 2006: Chemical Kinetics and Photochemical Data for Use in Atmospheric Studies, Evaluation No. 15, JPL Publication 06-2, Jet Propulsion Lab," 2006.

(5) NIST Chemistry WebBook, http://webbook.nist.gov/chemistry/, 2009.

(6) Cantrell, C. A.; Zimmer, A.; Tyndall, G. S. *Geophysical Research Letters* **1997**, *24*, 2195.

(7) Creasey, D. J.; Heard, D. E.; Lee, J. D. *Geophysical Research Letters* **2000**, *27*, 1651.

(8) FACSIMILE; 4.0.36 ed.; MCPA Software Ltd. 2002.

(9) Thiebaud, J.; Crunaire, S.; Fittschen, C. *Journal of Physical Chemistry A* **2007**, *111*, 6959.

(10) Andersson, B. Y.; Cox, R. A.; Jenkin, M. E. *Int. J. Chem. Kinetics* **1988**, *20*, 283.

(11) Christensen, L. E.; Okumura, M.; Hansen, J. C.; Sander, S. P.; Francisco, J. S. *Journal of Physical Chemistry A* **2006**, *110*, 6948.

(12) Christensen, L. E.; Okumura, M.; Sander, S. P.; Salawitch, R. J.; Toon, G. C.; Sen, B.; Blavier, J. F.; Jucks, K. W. *Geophysical Research Letters* **2002**, *29*.

(13) Stone, D.; Rowley, D. M. *Physical Chemistry Chemical Physics* **2005**, *7*, 2156.

(14) Tyndall, G. S., Orlando J. J., Personal communication.

(15) Fink, E. H.; Ramsay, D. A. *Journal of Molecular Spectroscopy* **1997**, *185*, 304.

(16) Freedman, P. A.; Jones, W. J. *Journal of the Chemical Society-Faraday Transactions Ii* **1976**, *72*, 207.

(17) Hunziker, H. E.; Wendt, H. R. *Journal of Chemical Physics* **1974**, *60*, 4622.

(18) Kanno, N.; Tonokura, K.; Tezaki, A.; Koshi, M. *Journal of Molecular Spectroscopy* **2005**, *229*, 193.

(19) DeSain, J. D.; Klippenstein, S. J.; Miller, J. A.; Taatjes, C. A. *Journal of Physical Chemistry A* **2003**, *107*, 4415.

(20) Tuckett, R. P.; Freedman, P. A.; Jones, W. J. *Molecular Physics* **1979**, *37*, 379.

(21) Johnson, T. J.; Wienhold, F. G.; Burrows, J. P.; Harris, G. W.; Burkhard, H. *Journal of Physical Chemistry* **1991**, *95*, 6499.

(22) Taatjes, C. A.; Oh, D. B. *Applied Optics* **1997**, *36*, 5817.